Boninites as Mercury lava analogues: geochemical and spectral measurements from pillow lavas on Cyprus island

N. Mari[1], G. L. Eggers[2], J. Filiberto[3], C. Carli[4], G. Pratesi[5], M. Alvaro[1], P. D'Incecco[6,7], M. Cardinale[6], G. Di Achille[6]

[1]Dipartimento di Scienze della Terra e dell'Ambiente, University of Pavia, Pavia, Italy. Corresponding author email: nicola.mari@unipv.it. [2]Lunar and Planetary Institute, USRA, Houston, TX, USA. [3]ARES XI3, NASA Johnson Space Center, Houston, TX, USA. [4]Istituto di Astrofisica e Planetologia Spaziali - INAF, Rome, Italy. [5]Museo di Scienze Planetarie, Prato, Italy. [6]National Institute for Astrophysics (INAF) - Astronomical Observatory of Abruzzo, Teramo, Italy. [7]Arctic Planetary Science Institute (APSI), Rovaniemi, Finland.

Abstract

In the absence of Mercurian rocks or meteorites in our collections, komatiites and boninites are often proposed as the best analogue rocks to Mercury lavas. However, despite previous work on the possible analogy between komatiites and Mercury rocks, similar work has not been done for boninites. In this work, we investigate the whole-rock geochemistry and visible/near-infrared (VNIR) spectroscopy of boninitic material collected at three specific areas of the Troodos Massif (Cyprus island). The objective is to evaluate if collected boninites, these along with other boninites present in the literature, can be analogous to Mercury geochemical terranes. On average, we find an unusually high MgO/SiO_2 ratio (0.68) for the boninites from the Troodos Massif compared with previous boninite analysis. This MgO/SiO_2 value is most closely related to the high-Mg regions of Mercury, while the average Al_2O_3/SiO_2 ratio (0.25) is consistent with the Mercurian intermediate terrain and to Mercury's largest pyroclastic deposit. In addition, further affinity to the high-Mg regions and the intermediate terrains of Mercury are shown in regard to Si vs. Mg, Si vs. Ca, and Si vs. Fe content for one sample in particular. We then conduct magmatic modeling on this specific sample to provide a possible parental melt composition for analogue Mercurian magmas. In

conclusion, we suggest these specific locations on the Troodos Massif in Cyprus as good geochemical analogue sites for the high-Mg regions of Mercury and explain how boninites could be important benchmark samples for the chemical and spectral data expected from the BepiColombo mission.

Keywords: Boninites, Mercury, Geochemistry, Lava, Planetary Analogue

1 – Introduction

Orbital dynamics in the Solar System is hostile to the delivery of Mercurian meteorites to Earth. In fact, the gravitational well of the Sun can easily circularize the orbit of any material that is ejected from the Mercury surface, destining the ejecta to re-impact Mercury (Melosh and Tonks 1993; Gladman et al. 1996; Dones et al. 1999). However, thanks to the NASA's - Mercury Surface, Space Environment, Geochemistry, and Ranging (MESSENGER) mission (e.g., Solomon et al., 2001; Solomon et al., 2018), we now know what a Mercurian meteorite (and, by consequence, Mercurian material in general) should look like (Love and Keil, 1995; McCubbin and McCoy, 2016).

Results from the X-Ray Spectrometer and Gamma-Ray and Neutron Spectrometer (Solomon et al., 2001) onboard the MESSENGER mission are in agreement with a Mercury surface composition containing a Mg/Si ratio that is in the range of terrestrial oceanic basalts and Moon basalts (0.33–0.67) and a very low Fe/Si ratio (0.03-0.15 or even lower, corresponding to 1-4 wt.% Fe) (Evans et al., 2012; Weider et al., 2012; Weider et al., 2015; Nittler et al., 2020). Mercurian materials from most regions also have lower Al/Si and Ca/Si than terrestrial and lunar basalts (Weider et al., 2015; McCoy and Nittler, 2014; Solomon et al., 2018; Nittler et al., 2020). Additionally, mineral phases as oldhamite and niningerite (which are present in highly reduced meteorites), along with an S concentration up to 4 wt.%, suggest that magmatic conditions on the surface of Mercury are extremely reduced and unique among terrestrial planets in the Solar System, reaching 6 to 3 log units below the Iron-Wustite (IW) buffer (Nittler et al., 2011: McCubbin et al., 2012; Namur et al., 2016; Zolotov et al., 2013).

Specifically, experimental petrology and modeling results show that the most appropriate rock for the intermediate terranes of Mercury should be a Mg-rich, Fe-poor basalt composed mainly of orthopyroxene and plagioclase (Stockstill-Cahill et al., 2012; Namur and Charlier, 2017; Vander Kaaden et al., 2017). Is there a way to establish which terrestrial material is analogue in terms of mineralogy and geochemistry to a Mercurian rock? Spectroscopy in the visible/near-infrared (VNIR) wavelengths is a powerful technique that can improve our mineralogical knowledge between acquired MESSENGER spectra and spectra measured from terrestrial minerals and rocks. Comparison of Mercury spectra with lunar material suggested that the surface of Mercury is dominated by pyroxene, Mg-rich olivine, and K-plagioclase (Jeanloz et al., 1995; Boynton et al., 2007; Warell et al., 2010; Solomon et al., 2018; Nittler et al., 2020). Previous VNIR measurements of analogue materials were conducted at both Mercury nighttime and daytime temperatures (approximately 500° C) since sulphides can thermally decompose below such daytime temperature, resulting in varied spectra (Helbert et al., 2013; Maturilli et al., 2014; Bott et al., 2023).

The most Mg-rich, Al-poor regions on Mercury, areas of suggested olivine- and plagioclase-rich lavas, have compositions and/or mineralogy analogous to terrestrial boninites, basaltic komatiites and komatiites (Charlier et al., 2013; Weider et al., 2015; Vander Kaaden et al., 2017; Namur and Charlier, 2017). Terrestrial komatiites and basaltic komatiites that may be analogues to Mercury have been investigated by Carli et al. (2013), while other komatiites were analyzed by Maturilli et al. (2014). Vander Kaaden and McCubbin (2016) discuss how the mechanism forming boninites on Mercury is different from the one on Earth, in the sense that they does not require hydrous melting. However, there has been no study on the spectral properties of terrestrial boninites from the point of view of their mineralogical analogy with Mercurian material.

Therefore, in this work, we not only investigate the whole-rock geochemistry but even the VNIR spectroscopy of a series of boninites of different composition that we collected on the island of Cyprus. These data are then discussed to see if the samples are applicable as new Mercury geochemical analogues and if they could be used as a benchmark for the expected geochemical analyses and spectra that will be acquired by the ESA/JAXA BepiColombo mission.

2 – Sample collection and geological setting

Samples of boninitic pillow lavas were collected by the main author on the Upper Pillow Lavas unit of the Troodos Massif, located on the island of Cyprus (Fig. 1, 2; Table 1). The Troodos Massif is made up of ophiolites generated by a particular phenomenon of suprasubduction-zone magmatism (Gass and Masson-Smith, 1963; Gass, 1967; Gass and Smewing, 1973). The ophiolite complex is composed of harzburgite, dunite, pyroxenite, gabbro, quartz diorite, diabase, and pillow lavas and formed in an old ridge of the Tethys paleo-ocean (e.g., Moores and Vine, 1971). The proposed parental melt for the Troodos ophiolite would be TiO_2- and Al_2O_3-poor and SiO_2-rich, with the most petrologically primitive lavas (enriched in MgO) present on the Upper Pillow Lavas unit (Cameron, 1985).

The Upper Pillow Lava unit of the Troodos ophiolite consists of boninites (Gass et al., 1994; Osozawa et al., 2012). Osozawa et al. (2012) found that the Lower Pillow Lavas unit, composed of tholeiites, erupted first, and was then followed by the eruption of boninites as the Upper Pillow Lava unit. Late infills of lava are composed of depleted boninites. In terms of Ar-Ar ages, the tholeiitic rocks were erupted 90.6 ± 1.2 Ma, followed by the eruption of boninitic lavas at ~75 Ma.

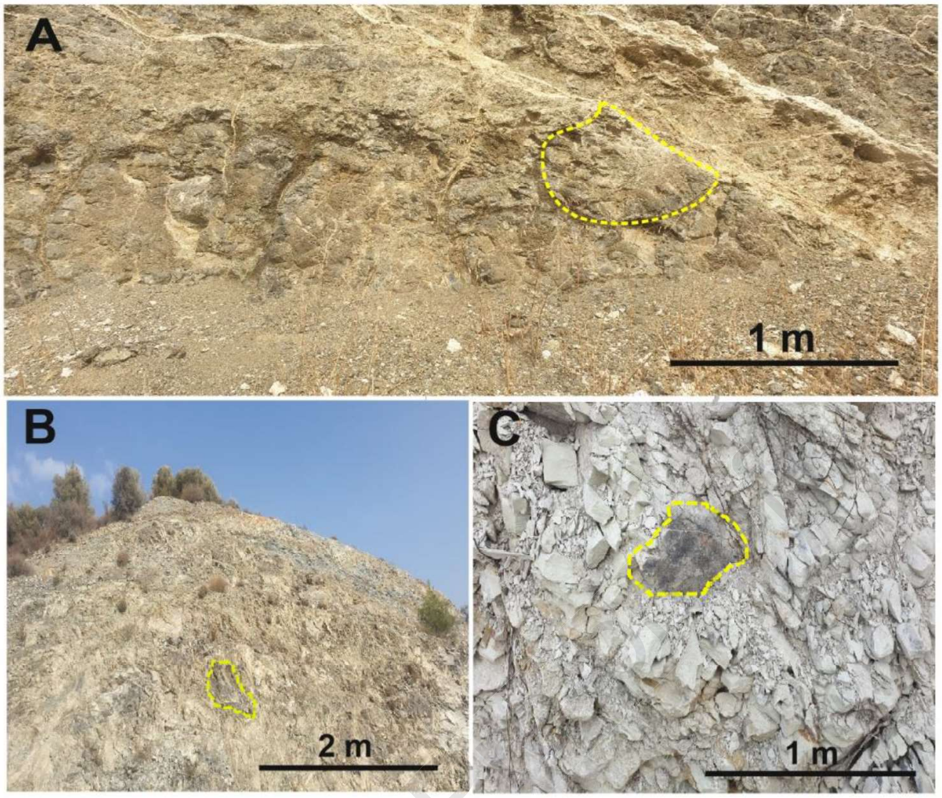

Figure 1 – Photos of the outcrops where the boninites were collected on Cyprus; see Table 1 for more information. A) Site in the Parekklisia area; B) site in the Kellaki area; C) site in the Asgata area. The yellow dashed curve is used to highlight the collection areas of the samples.

Table 1 – Information about the samples of boninite collected. Data on The Cyprus Geological Map are from Geological Survey Department Cyprus (1995) and Gass et al. (1994).

Sample Name	Place (location)	Lat - Coordinates (GPS)	Lon - Coordinates (GPS)
UPL 1	Parekklisia	34.75866384°	33.16136384°
UPL 2	Kellaki	34.79600339°	33.15288176°
UPL 3	Asgata	34.77172076°	33.24643589°

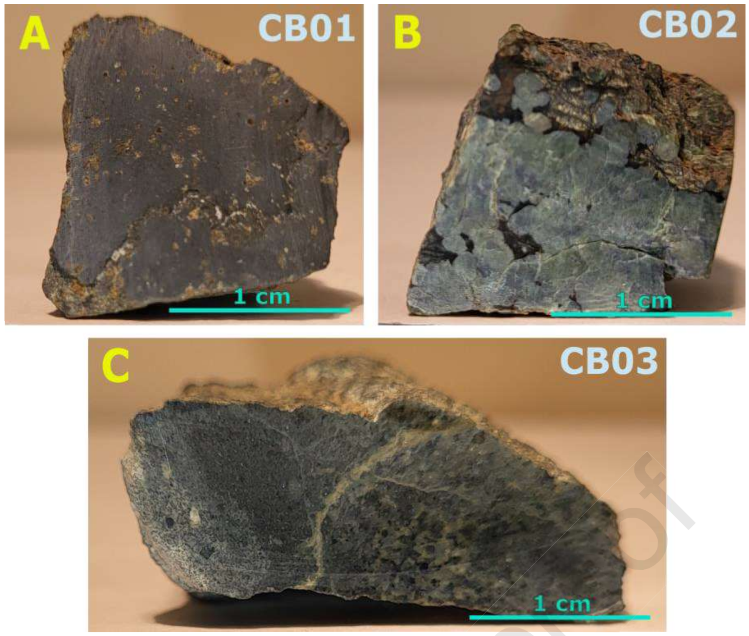

Figure 2 – Interior details of the samples that were analyzed using VNIR. A) CB01 (sample collected at UPL 1 site); B) CB02 (sample collected at UPL 2 site); C) CB03 (sample collected at UPL 3 site).

3 – Methods

The whole-rock geochemistry was acquired using a ShimadzuEDX-7000 equipped with a Rh source, located at the Centro di Servizi di Cristallografia Strutturale (CRIST) of the University of Firenze, with an Energy Dispersive X-ray Fluorescence (EDXRF) technique. The analyses were conducted in vacuum by analyzing a 10mm surface and with the scan that were conducted on both faces of each sample.

We measured VNIR reflectance of the boninite samples over the 0.35–2.5 µm range using a Spectral Evolution OreXpress SM-3500 spectrometer with its contact probe attachment, located at the Lunar and Planetary Institute, USRA. A standard white Spectralon plate (at 99%) was used as a reference. Spectra were collected in a dimly lit room and under a terrestrial atmosphere with illumination from a 5-watt tungsten halogen bulb internal to the probe and a rubber gasket surrounding the probe window. The spot size of the probe is ~10 mm and provides incidence and emission angles of ~0° and ~30°, respectively, with an overall phase angle of ~30°. The collected spectra are hyperspectral with nominal spectral resolutions of ≤ 3 nm (380–1000 nm), ≤ 10 nm (1000-1900 nm), and ≤ 7 nm (1900-2500 nm). Reflectance measurements were made on both the weathered, rough exteriors of each sample and their smooth interiors after being cut open to expose ideally less altered material. When collecting spectra of each sample, many measurements were taken of both the exterior and interior and compared, to see if they agreed well in terms of spectral shape and features.

We used the CIPW Norm (Cross et al., 1902) to extrapolate the proportions of pyroxene and olivine that are present in these boninite samples and that, by comparison, may be present in Mercurian rocks. Finally, we modeled the reverse fractional crystallization for expected Mercurian magmas at a log fO_2 of IW -6 (McCubbin et al., 2012; Namur et al., 2016; Zolotov et al., 2013). To do this modeling, we used the PetroGram software (Gündüz and Asan, 2021) and the PetroLog3 software (Danyushevsky and Plechov, 2011).

4 – Results

The macroscopic textures of each sample are varied (Fig. 2): CB01 is uniformly dark with no distinct crystals; CB02 has an abundance of large green crystals with some darker areas; and CB03 has mottled small black and white blocky crystals. As we can see from sample chips in Fig. 2 and from VNIR spectra in Fig. 3, these boninite samples are mainly composed of pyroxene and olivine. The CIPW normative minerals that we obtain when we use the whole-rock geochemistry of the boninite samples suggest dominant olivine in the CB02 sample (79.5 wt.% and 78.6 vol.% forsterite; 20.4 wt.% and 21.3 vol.% enstatite) with respect to sample CB01 (33.1 wt.% and 27.7 vol.% forsterite; 66.8 wt.% and 72.2 vol.% enstatite) and CB03 (56.2 wt.% and 53.7 vol.% forsterite; 43.7 wt.% and 46.2 vol.% enstatite). According to the classification of boninites from Le Bas (2000) and from Pearce and Reagan (2019) all three samples are considered low-Si boninites per the data in Table 2.

The whole-rock geochemistry for each sample (CB01, CB02, CB03) is reported in Table 2. The CB01 sample is more FeO-TiO_2-rich (18.83 wt.% and 0.42 wt.%, respectively) and MgO-poor (8.82 wt.%) than CB02 (2.31 wt.% FeO; 0.01 wt.% TiO_2; 44.64 wt.% MgO) and CB03 (3.71 wt.% FeO; 0.04 wt.% TiO_2; 32.82 wt.% MgO). Also, the CB01 sample is particularly enriched in CaO (11.52 wt.%). The CB02 sample is depleted in Al_2O_3 (2.93 wt.%) with respect to CB01 and CB03 (13.78 wt.% and 15.05 wt.%, respectively). These compositional differences among the three boninites analyzed here may be due to sampling bias in the Upper Pillow Lava unit in Cyprus.

Table 2 – Whole-rock geochemistry of the boninite samples collected via XRF analysis.

Wt.%	CB01	CB02	CB03
SiO_2	43.09	42.35	41.88
TiO_2	0.42	0.01	0.04
Al_2O_3	13.78	2.93	15.05
Cr_2O_3	0.27	0.18	0.08
MgO	8.82	44.64	32.82
CaO	11.52	7.36	6.09
MnO	1.59	0.11	0.05
FeO	18.83	2.31	3.71
K_2O	1.26	0.01	0.05
NiO	0.16	0.03	0.01
Total	99.74	99.93	99.78

Figure 3 provides representative spectra of both the exteriors and interiors of boninite samples CB01, CB02, and CB03 that bound the range of reflectance observed for each sample. A number of spectral features associated with primary rock mineralogy and alteration thereof are present. To be precise, sample CB01 exhibits major spectral absorptions at 1.002, 1.417, and 1.915 µm with weaker features at 2.245 and 2.316 µm. Sample CB02 shows major absorptions at 1.038, 1.393, and 1.906 µm with weaker features at 0.661 and 2.325 µm. Sample CB03 has major absorptions at 1.001, 1.422, and 1.911 µm with weaker features at 0.72, 1.802, 2.257, and 2.326 µm.

Spectra for the sample exteriors are relatively consistent with one another. All exhibit a broad ~1 μm band consistent with mafic mineralogy. However, all features also show strong and sharp ~1.4 μm and ~1.9 μm hydration bands associated with aqueous alteration. Alteration could also explain the minor features that appear in the ~0.65–0.7 μm and ~2.2–2.3 μm ranges.

To evaluate less altered material, the samples CB01, CB02, and CB03 were cut and spectra were taken of the interiors. Spectral features of alteration still appear in all interior samples, especially for CB02 (Fig. 3). However, those features are relatively weaker with respect to those from the same sample but acquired on the external face, and the interior spectra broadly exhibit lower reflectance, both suggesting less alteration. As for the exterior spectra, the interior spectra are all broadly consistent with one another, though the exact shape of the ~1 μm bands do vary, likely reflecting different mineral chemistry.

Serpentine minerals are the most likely alteration product present, accordingly to Kokaly et al. (2017). In sample CB02 especially, there is a good match for serpentine features at 1.29 and 2.32 μm, and feature at 1.9 μm, while indistinct, could match the broad, asymmetric absorption seen in serpentine minerals (Fig. 3b). Moreover, the CB02 sample itself features large green crystals that appear to be serpentine (Fig. 3b). As forsteritic olivine was present in the parent rock, serpentine is a reasonable alteration product.

Other alteration minerals present may include Fe-oxides, accordingly to Kokaly et al. (2017). While most Fe-oxides like hematite usually have spectral absorption features within the 0.8–0.9 μm range rather than the 0.65-0.7 μm feature present in samples CB02 and CB03, there are no other expected alteration minerals in this range. Fe-oxides are also supported by CB02, which exhibits visible rusty patches (Fig. 2b).

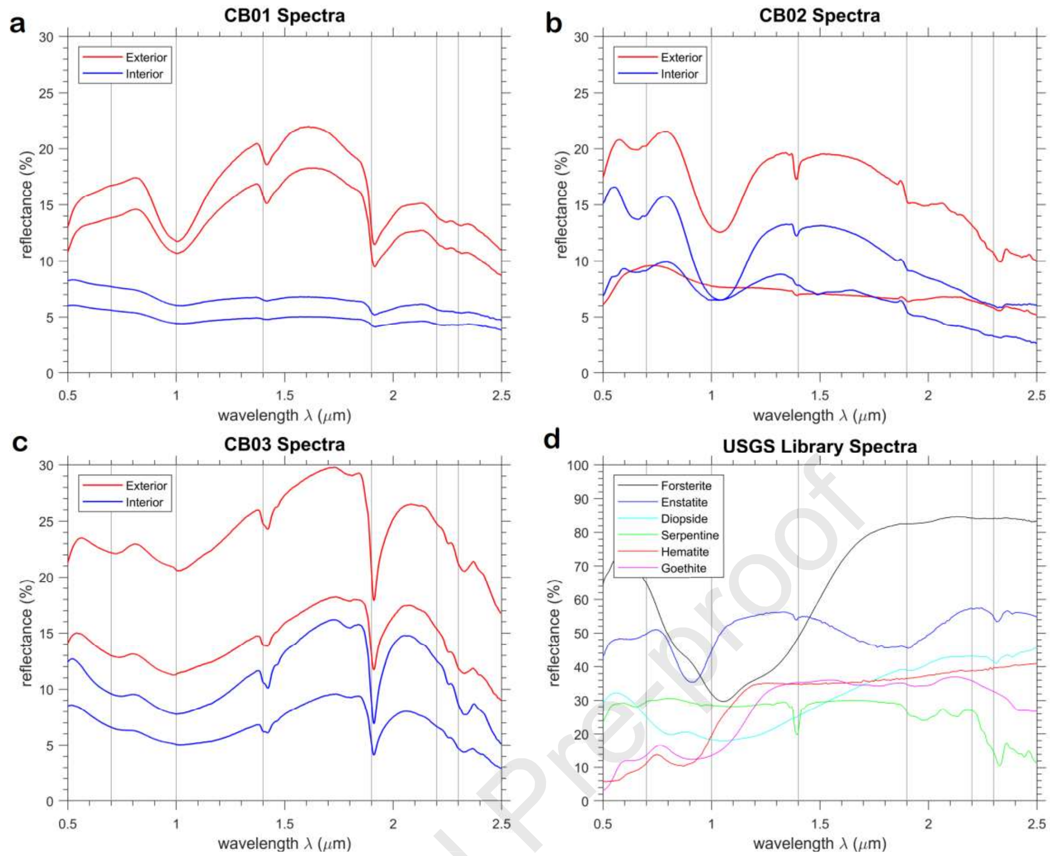

Figure 3 – VNIR spectra of the boninites. A) Sample CB01; B) Sample CB02; and C) Sample CB03. Representative spectra of both exteriors and cut interiors are plotted, demonstrating the approximate range in reflectances observed. D) Reference spectra from the USGS Spectral Library, for comparison to the boninite samples (Kokaly et al., 2017). Library spectra (with USGS ID) reproduced are forsterite (AZ-01), enstatite (NMNH128288), diopside (HS15.4B), serpentine (HS318.3B), hematite (FE2602), and goethite (GDS134), and absolute reflectances are converted to percent reflectance for comparison. For all panels, light gray guidelines are placed at 0.7, 1.4, 1.9, 2.2, and 2.3 µm.

5 – Discussion

Both the spectral data and the geochemical data on the boninites analyzed in this work reveal characteristics that are useful for the interpretation of expected spectra from Mercury mineralogy and the nature of the Mercury geochemical terranes. We start by discussing the VNIR data and then continue by focusing on the geochemistry aspect of these samples, including their analogy to Mercury.

5.1 – VNIR data interpretation

The VNIR reflectance spectra of the boninite samples show a mixture of primary igneous and alteration minerals. This is consistent with the fact that, when forming pillow lavas, the samples could inherit a certain degree of hydrothermal alteration (Humphris and Thompson, 1978). However, this alteration also complicates interpretation of the spectra and their application to Mercury.

The primary mineralogy of these samples is dominated by olivine, which is characterized by strong ~1 µm features (Fig. 3) (e.g., Burns, 1993). While olivine spectra of the samples often show broader, asymmetric features at slightly longer wavelengths, the Mg-rich olivine features more symmetrical bands shifted shortwards toward 1 µm due to lower iron content (Clark, 1999). Thus, in our case, forsteritic olivine is the better candidate. Sample CB03 has the strongest olivine signature, with its symmetrical 1 µm feature that extends to 1.7 µm.

The second primary mineral observed is orthopyroxene, which is typically identified by strong 1 and 2 µm features. However, these features can shift significantly, depending on Mg vs. Fe vs. Ca abundances. Relative to olivine, the 1 µm feature of orthopyroxene is narrower and symmetric, similar to the feature observed in CB01 and CB02 (Fig. 3a,b).

What is particularly important is the evidence that the absorption that we have from these spectra (in Fig. 3), with respect to the Mg enrichment of the mafic minerals, shows an higher capability to detect olivine and Ca-rich pyroxene, despite the abundance of orthopyroxene which is not negligible. This suggests that for the future spectra that will be acquired by SIMBIO-SYS onboard BepiColombo mission (Cremonese et al., 2020), if mineral assemblages could be similar (i.e., with a mafic component strongly enriched in Mg) to the studied boninites, we should expect a better definition of absorptions associated to olivine and high-Ca pyroxene. In fact, this could be used as an indication that even at such composition described in Table 2 – with 8.82 wt.% MgO for CB01; 44.64 wt.% MgO for CB02; and 32.82 wt.% MgO for CB03 - the absorption is present. Thus, materials attributable to mafic mineralogy with low amount of transitional elements, maybe having similar mineralogy as these boninites, could be highlighted, thanks to the higher spatial resolution and favorable geometry of acquisition, by the SIMBIO-SYS instrument (onboard BepiColombo). If these rocks should be suitable with boninites composition we should expect absorption band positions attributable to olivine and Ca-rich pyroxene taking into account the Band 1 of the spectra.

5.2 – Geochemical and magmatic comparison with Mercury

The composition information we have for the three analyzed boninite samples are compared with the different geochemical terranes of Mercury (Fig. 4) as reported by Vander Kaaden et al. (2017).

5.2.1 – Whole-rock geochemistry

Both the CB01 and the CB03 samples have an Al_2O_3 content (13.78 wt.% and 15.05 wt.%, respectively) that is similar to the intermediate terrane and the high-Al regions of Mercury (14.06 wt.%; Vander Kaaden et al., 2017) (Fig. 4a). In addition, the MgO abundance of the CB01 boninite (8.82 wt.%) is in common with the subset terrain of the low-Mg northern volcanic plains of Mercury and the Caloris Basin area, while the CB03 boninite has a Mg abundance (32.82 wt.%) typical of the high-Mg northern volcanic plains of Mercury. Basically, these two samples (CB01 and CB03) acts like endmembers for the Mg-content of the northern volcanic plains of Mercury (12.50 wt.% and 20.28 wt.%, respectively; Vander Kaaden et al., 2017). This can be seen also by looking at their SiO_2 vs. MgO and SiO_2 vs. CaO compositions (Fig. 4b,c).

By digging more into geochemical similarities between these boninites and Mercury, it is important to notice that the CB03 sample closely stands within the geochemistry of the intermediate terrains of Mercury even for its CaO- and FeO-content (6.09 wt.% CaO, 3.71 wt.% FeO for the boninite sample, Table 2; 5.74 wt.% CaO, 1.84 wt.% FeO for the Mercurian intermediate terrain, from Vander Kaaden et al., 2017). In addition, when we consider the total Fe + Ti versus Al versus Mg, we can see that sample CB03 exactly matches the composition of the High Mg regions and Rachmaninoff Basin (Fig. 5).

On the other hand, the CB02 boninite do not show an appreciable similarity in Mg-content with any of the Mercurian geochemical terrains (Fig. 4). However, both the CB02 and CB03 samples display a CaO (7.36 wt.% and 6.09 wt.%, respectively) and FeO (2.31 wt.% and 3.71 wt.%, respectively) content that closely resemble that of the high-Mg regions and the Rachmaninoff Basin, as well as the largest known Mercurian pyroclastic deposit (Fig. 4c,d).

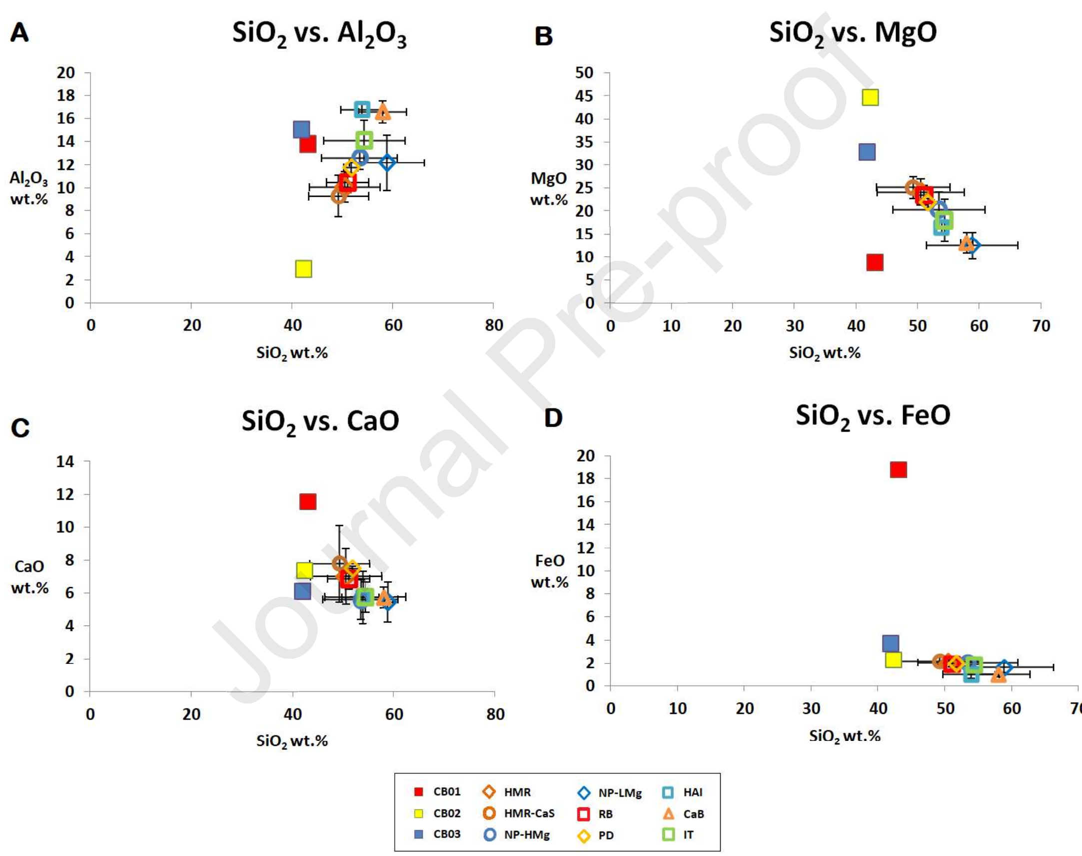

Figure 4 – Harker diagrams showing the geochemical comparison between the boninite samples from Cyprus (CB01, CB02, and CB03) and the geochemical terranes of Mercury (data from Vander Kaaden et al., 2017). Standard errors for the Mercury data are shown. Terranes plotted are the high-Mg region (HMR); high-Mg region with highest Ca and S (HMR-CaS); subset of the northern volcanic plains with high Mg (NP-HMg); subset of the northern volcanic plains with low Mg (NP-LMg); Rachmaninoff Basin (RB); Mercury's largest pyroclastic deposit (PD); the high-Al regions (HAl); Caloris Basin (CaB); and the intermediate terrane (IT).

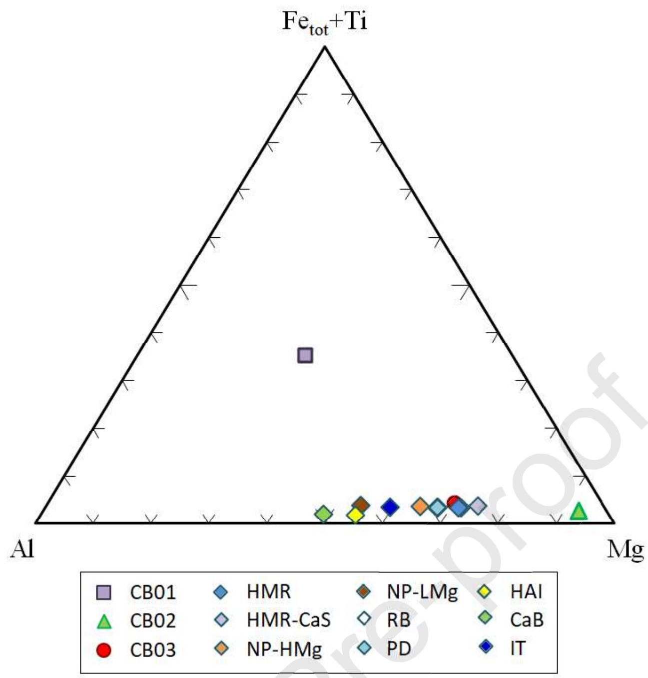

Figure 5 – Diagram showing the geochemical comparison for Fe+Ti versus Al versus Mg, between the boninite samples from Cyprus (CB01, CB02, and CB03), the Mercury geochemical terranes (data from Vander Kaaden et al., 2017). In this comparison, sample CB03 is most comparable to the high-Mg regions of Mercury, the Rachmaninoff Basin, and Mercury's largest pyroclastic deposit. Terranes plotted are the high-Mg region (HMR); high-Mg region with highest Ca and S (HMR-CaS); subset of the northern volcanic plains with high Mg (NP-HMg); subset of the northern volcanic plains with low Mg (NP-LMg); (RB); Mercury's largest pyroclastic deposit (PD); the high-Al regions (HAl); Caloris Basin (CaB); and the intermediate terrane (IT). Literature data from Pearce and Arculus (2021) and references therein. Diagram based on Jensen and Pyke (1982).

When we make a comparison between the boninites studied in this work with the main Mercurian geochemical terranes (Vander Kadeen et al., 2017) as well as boninite samples from representative areas of the Earth (Fig. 6), we find that the boninites collected on the Troodos Massif differ substantially in regards to the MgO/SiO_2 ratio, with the Troodos samples exhibiting a higher amount of MgO for the CB02 and CB03 samples, and a lower amount of Al_2O_3 for the CB02 sample. However, the CB01 sample is in agreement with the high-Al regions and the Caloris Basin of Mercury. The high Mg# is, however, within the range of boninites, which can feature a Mg/(Mg + Fe) of 0.55–0.83 (e.g., Hickey and Frey, 1982). In fact, we obtain a Mg/(Mg + Fe) of 0.77 for the boninites analyzed in this work. What we observe from the comparison in Figure 6 is that the Al_2O_3/SiO_2 ratio of these boninites from three specific locations of the Troodos Massif is different for each sample, especially for CB01 when is compared with CB02 and CB03, as we can also observe from Figure 4 for the CaO and FeO content. The MgO/SiO_2 ratio is, instead, higher than the Mercury geochemical terranes for CB02 and CB03; however, the CB03 sample is closer to the Mercury high-Mg regions (Fig. 6).

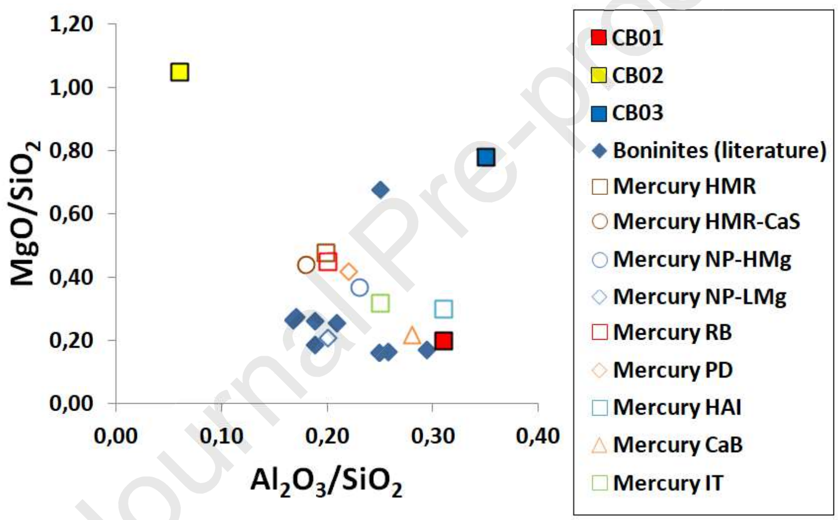

Figure 6 – Graph showing the ratio of Al_2O_3/SiO_2 versus MgO/SiO_2 for representative boninites from various locations, including the boninites from Troodos Massif studied in this work, in comparison with the representative Mercury geochemical terranes. The CB01 sample is the most representative for the high-Al regions and the Caloris Basin of Mercury. Two of the boninites analyzed in this work (CB02 and CB03) have an unusually high MgO/SiO_2 – where the CB03 can be related to the high-Mg regions of Mercury for its MgO/SiO_2 ratio – but the CB02 sample has a Al_2O_3/SiO_2 ratio lower than the average Mercury compositions, while the CB03 sample is consistent with the high-Al regions. Terranes plotted are the high-Mg region (HMR); high-Mg region with highest Ca and S (HMR-CaS); subset of the northern volcanic plains with high Mg (NP-HMg); subset of the northern volcanic plains with low Mg (NP-LMg); Rachmaninoff Basin (RB); Mercury's largest pyroclastic deposit (PD); the high-Al regions (HAl); Caloris Basin (CaB); and the intermediate terrane (IT). Boninite literature data are from Pearce and Arculus (2021) and references therein; Mercury geochemistry data is from Vander Kadeen et al. (2017).

To see what implication these boninite samples may have with regards to still unknown Mercurian volcanic rocks, we use the whole-rock geochemistry displayed in Table 2 to model magmatic processes in the following paragraphs.

5.2.2 – Magmatic modeling

The reverse fractional crystallization of these boninites could tell us more about possible magmatism on Mercury. Calculating the reverse of fractional crystallization is to add minerals that crystallized from a hypothetical melt back to the melt composition itself. In this way, the melt moves up along a cotectic, reaching primitive compositions (e.g., Hofmann and Feigenson, 1983). The whole-rock composition from each of the boninite samples (CB01, CB02, and CB03) was used as input for the calculation of the reverse fractional crystallization. For olivine- and orthopyroxene-melt equilibrium modeling, the model of Ariskin et al. (1993) was used. The starting pressure was set to 0.001 Kbar and the melt oxidation state was set to a log fO_2 of Iron-Wustite (IW) -6 (the maximum reducing condition for Mercury, according to McCubbin et al., 2012; Namur et al., 2016; Zolotov et al., 2013) and was calculated using methods from Borisov and Shapkin (1990). For calculating the melt physical characteristics, the chosen density model was based on Lange and Carmichael (1987) and the chosen viscosity model was based on Giordano and Dingwell (2003) and Vetere et al. (2017).

At 50% crystallization, we obtain a slightly different parental melt for the three boninite lavas, which altogether have an average density of 2.7 g/cm^3 and average viscosity of 31 poise. Here, we focus on the melt of the CB03 sample, which is the most interesting for a direct comparison with the high Mg regions of Mercury (see Fig. 4 and Fig. 5). By our calculations, this melt would have been enriched in SiO_2 and Al_2O_3 (41.77 wt.% and 30.17 wt.%, respectively) with significant amounts of MgO and CaO (10.81 wt.% and 12.21 wt.%, respectively), but poor in FeO and TiO_2 (4.58 wt.% and 0.08 wt.%, respectively), and with <0.5 wt.% amounts of MnO, K_2O, and CrO. This fall within the range of relative abundances of previous estimates for K_2O abundances (0.08-0.2 wt.%), for the parental melt composition of the Mercury lavas (mantle silicate composition) as hypothesized by Namur et al. (2016) after petrological experiments, especially in terms of and K_2O abundances; however, at 50% of crystallization, our calculation report higher amounts of SiO_2, FeO, TiO_2, Al_2O_3, MgO, and CaO in respect to the experimental results (52-58 wt.% SiO_2, 0.4 wt.% FeO, 0.4 wt.% TiO_2, 8.7-13.8 wt.% Al_2O_3, 13.9-27.8 wt.% MgO, and 5.8-7.2 wt.% CaO).

5.3 – Relevance for the BepiColombo mission and Mercury lava analogues

Along with the komatiites, the boninites (the ones analyzed in this work, along with those from the literature; see Fig. 6) should be considered as benchmark for the expected geochemical and spectral analysis that will be acquired by the SIMBIO-SYS/VIHI spectrometer (Cremonese et al., 2020) and MERTIS spectrometer (Hiesinger et al., 2020a,b) on board the ESA/JAXA BepiColombo mission (e.g., Benkhoff et al., 2021). For example, the boninite VNIR spectra collected in this work (Fig. 3) can be compared with spectra acquired from VIHI, where the same mineralogy - pyroxene and olivine - and, most important, extremely low similar fO_2 condition can be expected. In fact, spectra of extremely reduced assemblages may have specific characteristics (Burbine et al., 2002).

Constrained by the maximum reducing condition available on Earth, we can say that the CB03 boninite sample analyzed in this work is an acceptable new Mercury geochemical analogue that closely resembles the chemistry of the high Mg regions, considering its classification as a low-Si boninite, FeO and CaO composition, Fe-Ti-Al-Mg composition and Mg/SiO_2 ratio (Fig. 4; Fig. 5; Fig. 6); it has also a strong affinity with the Rachmanioff Basin and Mercury's largest pyroclastic deposit. In addition, we can see from Figure 6 that there are other boninites on Earth that may be useful as geochemical analogues of Mercury, by basing on MgO/SiO_2 and, especially, on Al_2O_3/SiO_2. In this sense, it is important to collect VNIR data also from other boninites to build a spectral dataset to compare to the data that will be acquired by BepiColombo.

Finally, it is important to say that a limit of this study is represented by the Mercury's environment itself. In fact, being an airless body by its nature, it is argued that the Mercurian surface is subject to space weathering and extreme temperatures that can modify properties of reflectance spectra (Maturilli et al., 2014; Brunetto et al., 2014; Lantz et al., 2017; Brunetto et al., 2020; Bott et al., 2023). Besides, it is important to understand that what is shown in this study will certainly not look exactly like what is found on Mercury because of the differences in the planetary environment. In addition, typical terrestrial chemical alterations detected in these boninite spectra (as for example, weathering) will very likely not be present on Mercury.

6 - Conclusion

The aim of this work was to investigate the whole-rock geochemistry and VNIR spectroscopy of boninites collected in different areas of the Troodos Massif (Cyprus) to see if the sample properties are relevant as Mercury terrain analogue. In light of our results, we argue for the following:

1) The CB01 boninite possess affinities with the high-Al regions, the northern volcanic plains with low Mg, and the Caloris Basin of Mercury, in terms of MgO/SiO_2 and Al_2O_3/SiO_2. However, this sample has higher FeO in respect to Mercury.

2) The parental melt of Mercurian volcanic rocks, as retrieved by our modeling, could have been enriched in SiO_2 and Al_2O_3, featured modest amounts of MgO and CaO, and depleted in FeO and TiO_2.

3) The CB03 boninite sample is a good geochemical and petrologic analogue for the high-Mg regions of Mercury.

4) The VNIR reflectance spectra for these boninites can be used as a benchmark to make a comparison with the future spectra that will be acquired from the VIHI instrument onboard the BepiColombo mission.

Acknowledgement

We acknowledge Dr. Christou Evangelos for his suggestions about the locations of sample collection on Cyprus.

Competing Interests Statement

The authors have no competing interests to declare.

References

Ariskin A. A., Barmina G. S., Frenkel M. Y. and Nielsen R. L., 1993. COMAGMAT: a Fortran program to model magma differentiation processes. *Computers and Geosciences*, vol. 19, pp. 1155–1170.

Benkhoff J., et al., 2021. BepiColombo - Mission Overview and Science Goals. *Space Sci. Rev*., vol. 217, issue 90.

Borisov A. A. and Shapkin A. I., 1990. A new empirical equation rating Fe^{3+}/Fe^{2+} in magmas to their composition, oxygen fugacity, and temperature. *Geochem. Int*., vol. 27, pp. 111–116.

Bott N., Brunetto R., Doressoundiram A., Carli C., Capaccioni F., Langevin Y., Perna D., Poulet F., Serventi G., Sgavetti M., Vetere F., Perugini D., Pauselli C., Borondics F. and Sandt C., 2023. Effects of Temperature on Visible and Infrared Spectra of Mercury Minerals Analogues. *Minerals*, vol. 13, issue 250.

Boynton W. V., et al., 2007. Concentration of H, Si, Cl, K, Fe, and Th in the low- and mid-latitude regions of Mars. *J. Geophys. Res.*, vol. 112, E12S99.

Brunetto R., Lantz C., Ledu D., Baklouti D., Barucci M. A., Beck P., Delauche L., Dionnet Z., Dumas P., Duprat J., Engrand C., Jamme F., Oudayer P., Quirico E., Sandt C. and Dartois E., 2014. Ion irradiation of Allende meteorite probed by visible, IR, and Raman spectroscopies. *Icarus*, vol. 237, pp. 278–292.

Brunetto R., Lantz C., Nakamura T., BakloutiD., Le Pivert-Jolivet T., Kobayashi S. and Borondics F., 2020. Characterizing irradiated surfaces using IR spectroscopy. *Icarus*, vol. 345, 113722.

Burbine T. H., McCoy T. J., Nittler L. R., Benedix G. K., Cloutis E. A. and Dickinson T. L., 2002. Spectra of extremely reduced assemblages: Implications for Mercury. *Meteoritics & Planetary Science*, vol. 37, pp. 1233–1244.

Burns R. G., 1993. Mineralogical Applications of Crystal Field Theory (second ed.), *Cambridge Univ. Press*, Cambridge, UK, p. 551.

Cameron W. E., 1985. Petrology and origin of primitive lavas from the Troodos ophiolite, Cyprus. *Contributions to Mineralogy and Petrology*, vol. 89, pp. 239–255.

Carli C., Serrano C. L. M., Maturilli A., Massironi M., Capaccioni F., and Helbert J., 2013. VNIR and TIR Spectra of Terrestrial Komatiites Possibly Analogues of some Hermean Terrain Compositions. *44th Lunar and Planetary Science Conference*. Abstract# 1923.

Charlier B., Grove T. L. and Zuber M. T., 2013. Phase equilibria of ultramafic compositions on Mercury and the origin of the compositional dichotomy. *Earth and Planetary Science Letters*, vol. 363, pp. 50-60.

Clark R. N., 1999. Spectroscopy of Rocks and Minerals, and Principles of Spectroscopy. In: A. N. Rencz (Ed.), *Remote sensing for the Earth sciences: Manual of remote sensing* (3rd ed., pp. 3– 52). John Wiley and Sons, Inc.

Cremonese G., et al., 2020. SIMBIO-SYS: Scientific Cameras and Spectrometer for the BepiColombo Mission. *Space Sci. Rev*., vol. 216, issue 75.

Cross W., Iddings J. P., Pirsson L. V. and Washington H. S., 1902. A quantitative chemico-mineralogical classification and nomenclature of igneous rocks. *Journal of Geology*, vol. 10, pp. 555–690.

Danyushevsky L. V. and Plechov P., 2011. Petrolog3: Integrated software for modeling crystallization processes. *Geochemistry Geophysics Geosystems*, vol. 12.

Dones L., Gladman B., Melosh H. J., Tonks W. B., Levison H.F. and Duncan M., 1999. Dynamical Lifetimes and Final Fates of Small Bodies: Orbit Integrations vs Öpik Calculations. *Icarus*, vol. 142, issue 2, pp. 509–524.

Evans L. G., Peplowski P. N., Rhodes E. A., Lawrence D. J., McCoy T. J., Nittler L. R., Solomon S. C., Sprague A. L., Stockstill-Cahill K. R., Starr R. D., Weider S. Z., Boynton W. V., Hamara D. K. and Goldsten J. O., 2012. Major-element abundances on the surface of Mercury: Results from the MESSENGER Gamma-Ray Spectrometer. *Journal of Geophysical Research*, vol. 117, E00L07.

Gass I. G. and Masson-Smith D., 1963, The geology and gravity anomalies of the Troodos Massif, Cyprus. *Royal Soc. London Philos. Trans. A*, vol. 255, pp. 417-467.

Gass I. G., 1967. The ultrabasic volcanic assemblage of the Troodos Massif, Cyprus. In: Wyllie, P. J., ed., Ultramafic and related rocks. *New York, John Wiley and Sons*, pp. 121-134.

Gass I. G. and Smewing J. D., 1973. Intrusion, extrusion, and metamorphism at constructive margins: evidence from the Troodos massif, Cyprus. *Nature*, vol. 242, pp. 26-29.

Gass I. G., MacLeod C. J., Murton B. J., Panayiotou A., Simonian K. O. and Xenophontos C., 1994. The Geology of the Southern Troodos Transform Fault Zone: Nicosia, Cyprus. *Geological Survey Department Cyprus, Ministry of Agriculture, Natural Resources and Environment, Government of Cyprus,* Memoir n. 9, 218 p.

Geological Survey Department Cyprus, 1995. Geological Map of Cyprus: Nicosia, Cyprus. *Ministry of Agriculture, Natural Resources and Environment, Government of Cyprus*, scale 1:250,000.

Giordano D. and Dingwell D., 2003. Viscosity of hydrous Etna basalt: implications for Plinian-style basaltic eruptions. *Bull. Volcanol*., vol. 65, pp. 8–14.

Gladman B. J., Burns J. A., Duncan M., Lee P. and Levison H. S., 1996. *Science*, vol. 271, pp. 1387–1392.

Gündüz M. and Asan K., 2021. PetroGram: An excel-based petrology program for modeling of magmatic processes. *Geoscience Frontiers*, vol. 12, issue 1, pp. 81-92.

Helbert J., Maturilli A. and D'Amore M., 2013. Visible and near-infrared reflectance spectra of thermally processed synthetic sulfides as a potential analog for the hollow forming materials on Mercury. *Earth and Planetary Science Letters*, vol. 369-370, pp. 233-238.

Hickey R. L. and Frey F. A., 1982. Geochemical characteristics of boninite series volcanics: implications for their source. *Geochimica et Cosmochimica Acta*, vol. 46, issue 11, pp. 2099-2115.

Hiesinger H., et al., 2020a. Studying the Composition and Mineralogy of the Hermean Surface with the Mercury Radiometer and Thermal Infrared Spectrometer (MERTIS) for the BepiColombo Mission: An Update. *Space Sci. Rev*., vol. 216, issue 110.

Hiesinger H., et al., 2020b. Correction to: Studying the Composition and Mineralogy of the Hermean Surface with the Mercury Radiometer and Thermal Infrared Spectrometer (MERTIS) for the BepiColombo Mission: An Update. *Space Sci. Rev*., vol. 216, issue 147.

Hofmann A. W. and Feigenson M. D., 1983. Case studies on the origin of basalt. *Contr. Mineral. and Petrol*., vol. 84, pp. 382–389.

Humphris S. E. and Thompson G., 1978. Hydrothermal alteration of oceanic basalts by seawater. *Geochimica et Cosmochimica Acta*, vol. 42, issue 1, pp. 107-125.

Jeanloz R., Mitchell D. L., Sprague A. L. and de Pater I., 1995. Evidence for a Basalt-Free Surface on Mercury and Implications for Internal Heat. *Science*, vol. 268, issue 5216, pp. 1455–1457.

Jensen L. R. and Pyke D. R., 1982. Komatiites in the Ontario portion of the Abitibi belt. In: Komatiites, Arndt N. T. and Nisbet E. G. Eds., *Allen and Unwin*, London.

Kokaly R. F., Clark R. N., Swayze G. A., Livo K. E., Hoefen T. M., Pearson N. C., Wise R. A., Benzel W. M., Lowers H. A., Driscoll R. L. and Klein A. J., 2017. USGS Spectral Library Version 7 Data. *U.S. Geological Survey data release.*

Lange R. A. and Carmichael I. S. E., 1987. Densities of Na2O-K2O-CaO-MgO-FeO-Fe2O3- Al2O3-TiO2-SiO2 liquids: New measurements and derived partial molar properties. *Geochimica et Cosmochimica Acta*, vol. 51, pp. 2931-2946.

Lantz C., Brunetto R., Barucci M. A., Fornasier S., Baklouti D., Bourçois J. and Godard M., 2017. Ion irradiation of carbonaceous chondrites: A new view of space weathering on primitive asteroids. *Icarus*, vol. 285, pp. 43-57.

Le Bas M. J., 2000. IUGS Reclassification of the High-Mg and Picritic Volcanic Rocks. *Journal of Petrology*, vol. 41, issue 10, pp. 1467–1470.

Love S. G. and Keil K., 1995. Recognizing mercurian meteorites. *Meteorit. Planet. Sci*., vol. 30, pp. 269–278.

Maturilli A., Helbert J., St. John J. M., Head J. W., Vaughan W. M., D'Amore M., Gottschalk M. and Ferrari S., 2014. Komatiites as Mercury surface analogues: Spectral measurements at PEL. *Earth and Planetary Science Letters*, vol. 398, pp. 58-65.

McCoy T. J. and Nittler L. R., 2014. Mercury. In: *Planets, Asteriods, Comets and The Solar System (Vol. 2), Treatise on Geochemistry (Second Edition, eds: H. D. Holland and K. K. Turekian)*. Oxford: Elsevier-Pergamon, pp. 119-126.

McCubbin F. M., M. A. Riner, K. E. Vander Kaaden, and L. K. Burkemper, 2012. Is Mercury a volatile-rich planet? *Geophysical Research Letters*, vol. 39, issue 9.

McCubbin F. M. and McCoy T. J., 2016. Expected Geochemical and Mineralogical Properties of Meteorites From Inferences From MESSENGER Data. *79th Meteoritical Society Meeting*, Abstract# 6242.

Melosh H. J. and Tonks W. B., 1993. Swapping Rocks: Ejection and Exchange of Surface Material Among the Terrestrial Planets. *Meteoritics*, vol. 28, issue 3, pp. 398-398.

Moores E. M. and Vine F. J., 1971. The Troodos Massif, Cyprus and other ophiolites as oceanic crust: evaluation and implications. *Royal Soc. London Philos. Trans. A*, vol. 268, pp. 443-466.

Namur O., Collinet M., Charlier B., Grove T. L., Holtz F. and McCammon C., 2016. Melting processes and mantle sources of lavas on Mercury. *Earth Planet. Sci. Lett*., vol. 439, pp. 117–128.

Namur O. and Charlier B., 2017. Silicate mineralogy at the surface of Mercury. *Nature Geoscience*, vol. 10, pp. 9–13.

Nittler L. R., Frank E. A., Weider S. Z., Crapster-Pregont E., Vorburger A., Starr R. D. and Solomon S. C., 2020. Global major-element maps of Mercury from four years of MESSENGER X-Ray Spectrometer observations. *Icarus*, vol. 345, 113716.

Osozawa S., Shinjo R., Lo C. -H., Jahn B., Hoang N., Sasaki M., Ishikawa K., Kano H., Hoshi H., Xenophontos C., and Wakabayashi J., 2012. Geochemistry and geochronology of the Troodos ophiolite: An SSZ ophiolite generated by subduction initiation and an extended episode of ridge subduction?. *Lithosphere*, vol. 4, issue 6, pp. 497-510.

Pearce J. A. and Reagan M. K., 2019. Identification, classification, and interpretation of boninites from Anthropocene to Eoarchean using Si-Mg-Ti systematics. *Geosphere,* vol. 15, issue 4, pp. 1008–1037.

Pearce J. A. and Arculus R. J., 2021. Boninites. In: Encyclopedia of Geology (Second Edition), Editor(s): David Alderton, Scott A. Elias. *Academic Press*, pp. 113-129, ISBN 9780081029091.

Solomon S. C., Nittler L. R. and Anderson B. J., 2018. Mercury: the view after MESSENGER. *Cambridge University Press*, 583 p.

Solomon S. C., et al., 2001. The MESSENGER mission to Mercury: scientific objectives and implementation. *Planetary and Space Science*, vol 49, issues 14–15, pp. 1445-1465.

Stockstill-Cahill K. R., McCoy T. J., Nittler L. R., Weider S. Z. and Hauck II S. A., 2012. Magnesium-rich crustal compositions on Mercury: Implications for magmatism from petrologic modeling. *J. Geophys. Res*., vol. 117, E00L15.

Vander Kaaden K. E. and McCubbin F. M., 2016. The origin of boninites on Mercury: An experimental study of the northern volcanic plains lavas. *Geochimica et Cosmochimica Acta*, vol. 173, pp. 246–263.

Vander Kaaden K. E., McCubbin F. M., Nittler L. R., Peplowski P. N., Weider S. Z., Frank E. A. and McCoy T. J., 2017. Geochemistry, mineralogy, and petrology of boninitic and komatiitic rocks on the mercurian surface: Insights into the mercurian mantle. *Icarus*, vol. 285, pp. 155-168.

Vetere F., Rossi S., Namur O., Morgavi D., Misiti V., Mancinelli P., Petrelli M., Pauselli C., and Perugini D., 2017. Experimental constraints on the rheology, eruption, and emplacement dynamics of analog lavas comparable to Mercury's northern volcanic plains. *Journal of Geophysical Research: Planets*, vol. 122.

Warell J., Sprague A., Kozlowski R., Rothery D. A., Lewis N., Helbert J., and Cloutis E., 2010. Constraints on Mercury's surface composition from MESSENGER and ground-based spectroscopy. *Icarus*, vol. 209, issue 1, pp. 138-163.

Weider S. Z., Nittler L. R., Starr R. D., McCoy T. J., Stockstill-Cahill K. R., Byrne P. K., Denevi B. W., Head J. W. and Solomon S. C., 2012. Chemical heterogeneity on Mercury's surface revealed by the MESSENGER X-Ray Spectrometer. *Journal of Geophysical Research*, vol. 117, E00L05.

Weider S. Z., Nittler L. R., Starr R. D., Crapster-Pregont E. J., Peplowski P. N., Denevi B. W., Head J. W., Byrne P. K., Hauck S. A., Ebel D. S., and Solomon S. C., 2015. Evidence for geochemical terranes on Mercury: Global mapping of major elements with MESSENGER's X-Ray Spectrometer. *Earth and Planetary Science Letters*, vol. 416, pp. 109-120.

Zolotov M. Y., Sprague A. L., Hauck II S. A., Nittler L. R., Solomon S. C., and Weider S. Z., 2013. The redox state, FeO content, and origin of sulfur-rich magmas on Mercury. *Journal of Geophysical Research: Planets*, vol. 118, pp. 138–146.

- The geochemistry and VNIR spectroscopy of boninitic material is investigated

- An high MgO/SiO_2 ratio (0.68) for the boninites from the Troodos Massif is reported

- Boninites from Cyprus are good geochemical analogues for the high-Mg terrains of Mercury

The author ensure that contributions of all authors are correct, and that all authors contributed to the editing and the revision of the manuscript.

Declaration of interests

☒ The authors declare that they have no known competing financial interests or personal relationships that could have appeared to influence the work reported in this paper.

☐ The authors declare the following financial interests/personal relationships which may be considered as potential competing interests: